Physically-Based Post-Processing Framework for Emulating Analog Color Photography

Daiki Nakajima

Abstract—The analog photography aesthetic has seen a resurgence in contemporary photography, with many artists seeking to reproduce the distinctive look of film. However, shooting on physical film remains expensive and challenging for amateurs, leading many photographers to the post-processing of digital images to achieve the analog look. Common existing approaches are either oversimple and fail to capture the aesthetic, or require laborious per-image adjustment that does not generalize across different projects. To address these challenges, we present a physically grounded post-processing pipeline that emulates the darkroom process. Our work builds on an open-source software [1]; we provide a formal mathematical treatment of this pipeline, deriving each stage from physical principles.

Index Terms—Computational Photography, Physical Simulation, Theory of Color

1 Introduction

The aesthetic of analog color photography has experienced a renewed interest in contemporary culture. Images captured on film exhibit distinctive visual qualities such as characteristic color reproduction, nonlinear tonal response, halation, and film grain, that is desirable for many photographers and artists. Despite this demand, capturing images directly on physical film remains costly and technically demanding for many practitioners. Film stocks are limited in availability, development requires specialized equipment or professional laboratories, and the process itself provides less immediate feedback than digital workflows. Consequently, many photographers attempt to recreate the analog aesthetic through digital post-processing.

Two common post-processing approaches include the use of preset filters (e.g. Instagram filters) or manual post-processing (e.g. Photoshop). Unfortunately, preset filters are often too simplistic and fail to capture the distinctive analog look that arises from complex photochemistry of the darkroom process. On the other hand, while manual post-processing can produce compelling results, these approaches typically involve heuristic adjustments of various parameters which can be time-consuming and do not generalize across different projects.

In traditional analog color photography, the final image is produced through a multi-stage process involving exposure of a multilayer color negative, chemical development of silver-halide grains and dye couplers, and optical printing onto photographic paper. Each stage introduces nonlinear transformations in color and density, interactions between color layers, and stochastic effects such as grain formation. These processes are governed by the physical properties of the film stock, the spectral sensitivity of the emulsion layers, and the response curves of both the negative and the print paper. Accurately reproducing the visual qualities of film therefore requires modeling not just the final tonal response but the underlying image-formation pipeline.

In this work, we present a physically grounded post-processing method that emulates the appearance of analog color film from a digital input image. Our approach models key stages of the photographic pipeline, including negative exposure and the printing process onto photographic paper. By leveraging publicly available data on popular film stock negatives and print papers, the method captures the nonlinear color interactions and tonal compression inherent to film photography.

Fig. 1: **Emulating the Analog Look:** Given an input digital image (top left), our method emulates the exposure and development of a color negative (top right), followed by the optical printing stage to produce the final film-like image (bottom).

Fig. 2: **Visualization of the Pipeline:** Given an input RGB image and data for a chosen film negative and photographic paper, the pipeline applies a series of effects to the image to obtain a processed negative. Then, we emulate the printing process to obtain the final image. (Note that some color spaces were inverted and/or adjusted for visualization.)

2 Related Work

The image-formation pipeline of a camera has been studied extensively in computer graphics. [2] introduced a physically-based camera model in which a lens system is described as a sequence of simple elements. [3] describes a simulation of the full digital camera processing chain and validates it against measured sensor data.

Image manipulation and style transfer is explored extensively in machine learning. [4] is an early exploration, on which later works expand on by applying more sophisticated deep learning algorithms for color correction and tone enhancement [5], [6], convolutional neural networks for style transfer [7], [8], and real-time stylization [9].

Film grain is one of the most identifiable and sought-after elements of film photography. [10] proposes a resolution-independent film-grain rendering algorithm based on a physically motivated stochastic model of the silver-halide process. Grains are represented as an inhomogeneous Boolean model of disks, and a Monte Carlo algorithm evaluates each output pixel at any desired resolution. A companion paper [11] further expands on the implementation details of this stochastic model. Our grain model uses a simplified Poisson–binomial approximation that retains the key density-dependent statistics of these models while remaining tractable for full-image simulation.

As for complete end-to-end simulation pipelines of analog film photography, an early work is given by [12], who model monochrome print making using quantitative descriptions of density response, spectral sensitivity, resolution, and granularity. However, their work is strictly for black-and-white images and does not consider color photography. [13] presents a physically and chemically based framework for simulating alternative photographic processes. They propose two approaches: (1) a fluid simulation pipeline to directly simulate the transport and reaction of chemicals in the emulsion using a Lattice Boltzmann solver, and (2) a data-driven approach based on characteristic curves that approximates the tonal response of photographic materials. While their first method achieves compelling results, it is complex and assumes a GPU implementation for efficiency. Our approach takes insight from their second approach, utilizing characteristic curves.

Recently, [1] released an open-source implementation that models analog color photography by simulating both the negative exposure and positive print stages, including development-inhibitor-releasing (DIR) couplers [14], [15] as a key mechanism for controlling color saturation. This attracted some attention in the photography community; however, no formal technical documentation of the methodology exists. Our work is largely based on their implementation, and serves to formalize and document the underlying model with rigorous mathematical descriptions and physical justifications.

On the commercial side, Dehancer [16] is a high-quality proprietary film-emulation plug-in integrated into widely used image- and video-editing software such as Adobe Photoshop, Adobe Premiere Pro, and DaVinci Resolve. While Dehancer produces top-quality results, it is closed-source and its methodology is not publicly available.

3 Film Exposure and Development

Starting from a linear RGB image, we model the darkroom process in two stages: the negative stage, and the paper printing stage. Here we cover the negative stage.

3.1 Spectral Upsampling

Physical simulation requires a per-wavelength representation of scene radiance; the three-channel RGB image provides an insufficient basis for modelling wavelength-dependent chemical sensitivities. Following [17], we lift each pixel's linear RGB color representation $\mathbf{c} \in \mathbb{R}^3$ to a spectral distribution using their precomputed basis $\mathbf{B} \in \mathbb{R}^{L\times 3}$, where L is the number of spectral samples.

Before projection, the basis is weighted by the film's reference illuminant $\mathbf{e} \in \mathbb{R}^L$ to account for the spectral power of the light source under which the scene is assumed to be viewed:

$$\tilde{\mathbf{B}} = \mathbf{B} \odot (\mathbf{e}\,\mathbf{1}^\top), \qquad \tilde{\mathbf{B}} \in \mathbb{R}^{L\times 3}, \tag{1}$$

where $\odot$ denotes element-wise multiplication. The per-pixel raw spectral signal is then

$$\mathbf{r}_{ij} = \tilde{\mathbf{B}}\,\mathbf{c}_{ij}, \qquad \mathbf{r}_{ij} \in \mathbb{R}^L. \tag{2}$$

The result is normalized so that an 18% mid-grey patch ($\mathbf{c} = 0.184\,\mathbf{1}$) produces unit response in the green emulsion layer:

$$\hat{\mathbf{r}}_{ij} = \frac{\mathbf{r}_{ij}}{0.184\,(\mathbf{e}^\top \mathbf{s}_{\text{green}})}, \tag{3}$$

where $\mathbf{s}_{\text{green}} \in \mathbb{R}^L$ is the spectral sensitivity of the green emulsion layer after UV/IR filtering.

3.2 Camera Exposure and Film Sensitometry

3.2.1 Auto-exposure

An auto-exposure compensation E_v is computed to place the median scene luminance $\bar{Y}$ at the 18% grey point:

$$E_v = -\log_2\left(\frac{\bar{Y}}{0.184}\right). \tag{4}$$

A user-input exposure offset can be added to this value for more creative control.

3.2.2 UV/IR cut-off filter

The film's base spectral sensitivity $s_k^0(\lambda)$ is attenuated by a UV/IR cut-off filter before any exposure calculations:

$$f_{\text{UV}}(\lambda) = 1 - a_{\text{UV}} + a_{\text{UV}}\,\Phi\left(\frac{\lambda - \lambda_{\text{UV}}}{\sigma_{\text{UV}}}\right), \tag{5a}$$

$$f_{\text{IR}}(\lambda) = 1 - a_{\text{IR}} + a_{\text{IR}}\,\Phi\left(\frac{\lambda_{\text{IR}} - \lambda}{\sigma_{\text{IR}}}\right), \tag{5b}$$

$$f_{\text{UV/IR}}(\lambda) = f_{\text{UV}}(\lambda)\cdot f_{\text{IR}}(\lambda), \tag{5c}$$

where $\Phi(x) = \frac{1}{2}[1 + \operatorname{erf}(x)]$ is the standard normal cumulative distribution function. For each filter, $a_{\text{UV/IR}} \in [0,1]$ specifies the attenuation strength, $\lambda_{\text{UV/IR}}$ denotes the central wavelength of the transition region, and $\sigma_{\text{UV/IR}}$ controls the smoothness of the cutoff. The filtered sensitivity is $s_k(\lambda) = s_k^0(\lambda)\, f_{\text{UV/IR}}(\lambda)$.

3.2.3 Spectral film exposure

Let indices (i,j) denote the pixel row and column, and $k \in \{C, M, Y\}$ denote the emulsion layer. The per-pixel raw film exposure for layer k is obtained by projecting the normalized spectral radiance $\hat{\mathbf{r}}$ onto the filtered sensitivity of each emulsion layer:

$$R_{ijk} = 2^{E_v} \int_{\Lambda} \hat{r}_{ij}(\lambda)\, s_k(\lambda)\, \mathrm{d}\lambda, \tag{6}$$

where $\Lambda = [380, 780]$ nm denotes the visible electromagnetic spectrum. In our implementation, all spectral integrals are evaluated on a uniform grid with $\Delta\lambda = 5$ nm.

3.2.4 Halation and grain scattering

Each layer channel undergoes two independent scatter passes that model

1) *Halation*: light that reflects off the film base and re-exposes the emulsion from behind, causing bright highlights to bloom into neighbouring regions.
2) *Subsurface grain scattering*: light that diffuses laterally in the emulsion before absorption by silver-halide grains.

Each pass blends the channel with a Gaussian-blurred copy of itself:

$$R_{\text{out}}^{(k)} = \frac{R^{(k)} + \alpha\, G_\sigma * R^{(k)}}{1 + \alpha}. \tag{7}$$

The two passes use independent radii $(\sigma_h^{(k)}, \sigma_s^{(k)})$ and strengths $(\alpha_h^{(k)}, \alpha_s^{(k)})$ per emulsion layer k.

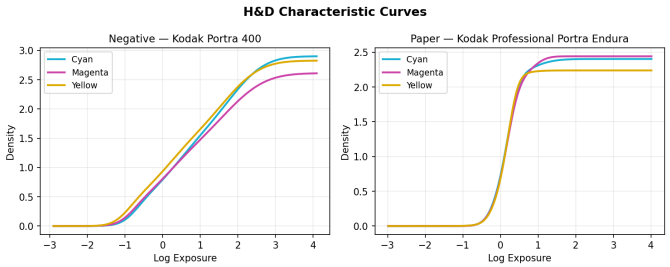

Fig. 3: **H&D characteristic curves.** Nonlinear profiles for a Kodak Portra 400 film negative (left) and Kodak Professional Portra Endura photographic paper (right), giving unique film- and paper-specific color mappings.

3.3 Characteristic Curve (H&D) Mapping

The log-exposure image $H_{ijk} = \log_{10} R_{ijk}$ is mapped to optical density via the Hurter–Driffield (H&D) characteristic curve [18], [19]. For each emulsion layer k, the curve $D_k : \mathbb{R} \to \mathbb{R}_{\geq 0}$ is stored as a look-up table over a calibrated log-exposure axis $\mathcal{E}$ and applied by linear interpolation:

$$d_{ijk} = D_k\left(\frac{H_{ijk}}{\gamma_k}\right), \tag{8}$$

where $\gamma_k > 0$ is a per-channel scale factor that stretches or compresses the log-exposure axis, effectively controlling the tonal range of each layer. The density floor is normalized to zero by subtracting $\min_j D_k(\mathcal{E}_j)$ from each curve.

3.4 DIR-Coupler Inhibition

Development-inhibitor-releasing (DIR) couplers are chemical agents in color-negative emulsions that release inhibitor molecules during development [14], [15]. These molecules diffuse laterally and between layers and can control the overall saturation of the output image.

3.4.1 Inhibition matrix

Inter-layer coupling is modeled by a 3×3 inhibition matrix $\mathbf{M}$. A Gaussian smoothing with standard deviation σ_ℓ is applied along the column axis to distribute each layer's inhibition across neighboring layers:

$$\tilde{M}_{jk} = \left(G_{\sigma_\ell} *_{\text{col}} \mathbf{I}_3\right)_{jk}, \tag{9a}$$

$$M_{jk} = \alpha_j \frac{\tilde{M}_{jk}}{\sum_{k'} \tilde{M}_{jk'}}, \tag{9b}$$

where $\alpha_j \geq 0$ is the inhibition strength of layer j. The normalization in Eq. (9b) is taken over columns k' so that each row sums to α_j: the total inhibition released by layer j is α_j, distributed across layers.

3.4.2 Curve adjustment for global inhibition

The H&D curves are shifted along the log-exposure axis to model the average inhibition field. A normalized highlight-boost density is first computed at each calibrated-axis step:

$$\hat{d}_{jk} = \frac{D_k(\mathcal{E}_j)}{D_k^{\max}} + \beta\left(\frac{D_k(\mathcal{E}_j)}{D_k^{\max}}\right)^2, \tag{10}$$

Fig. 4: **The Effect of DIR Couplers:** As the amount of DIR couplers increases, the resulting image becomes more saturated.

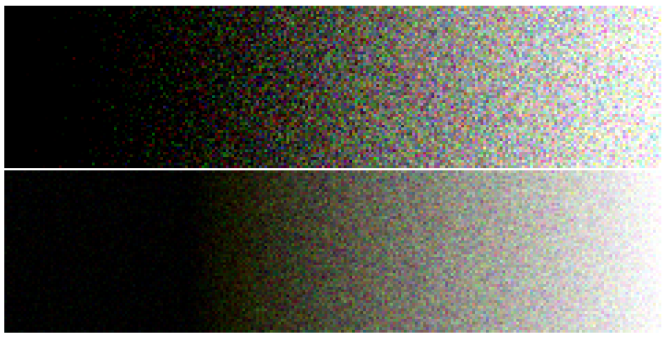

Fig. 5: **Grain Comparison:** A common approach to simulating grain is to overlay white noise on the image (top). However, this produces grain with uniform statistics across shadows and highlights. A Poisson–binomial grain model produces density-dependent grain that varies with image exposure (bottom).

where $D_k^{\max} = \max_{j'} D_k(\mathcal{E}_{j'})$ and $\beta \geq 0$ is a user-input highlight-boost parameter. The inhibition-adjusted log-exposure for channel m is

$$\tilde{\mathcal{E}}_{jm} = \mathcal{E}_j - \sum_k \hat{d}_{jk}\, M_{km}, \tag{11}$$

and the corrected curve $\tilde{D}_m$ is obtained by re-interpolating D_m from $\mathcal{E}$ onto $\tilde{\mathcal{E}}_{\cdot m}$.

3.4.3 Spatial inhibition

A spatially varying inhibition field is derived from the current per-pixel density image $\mathbf{d} \in \mathbb{R}^{H\times W\times 3}$. The per-pixel analog of Eq. (10) gives

$$\hat{d}_{ijk} = \frac{d_{ijk}}{D_k^{\max}} + \beta\left(\frac{d_{ijk}}{D_k^{\max}}\right)^2. \tag{12}$$

These per-layer normalized densities are projected through the inhibition matrix; the result is then convolved with a blurring kernel to model lateral diffusion:

$$F_{ijm} = G_{\sigma_d} * \left[\sum_k \hat{d}_{ijk}\, M_{km}\right], \tag{13}$$

where σ_d is the lateral diffusion radius. The log-exposure is corrected pixel-wise and the adjusted curves are applied:

$$\tilde{H}_{ijk} = H_{ijk} - F_{ijk}, \qquad d_{ijk} = \tilde{D}_k\left(\frac{\tilde{H}_{ijk}}{\gamma_k}\right). \tag{14}$$

3.5 Photographic Grain Simulation

Silver-halide grain is simulated independently for each CMY emulsion layer using a Poisson–binomial stochastic process [20], [21]. The expected number of developable grains per pixel in layer k is

$$N_k = \frac{p_x^2}{A_{\text{particle}}\,\rho_k}, \tag{15}$$

where p_x is the pixel pitch in µm, A_{particle} is the mean grain particle area, and ρ_k is a per-channel scale factor.

Working density is offset by a base-density floor $d_k^{\min}$; the per-pixel development probability is

$$p_{ijk} = \text{clip}\left(\frac{d_{ijk} + d_k^{\min}}{D_k^{\max} + d_k^{\min}},\ \varepsilon,\ 1-\varepsilon\right), \tag{16}$$

where $D_k^{\max}$ is the curve maximum. A saturation factor suppresses over-development at high densities, modeling competition between grains for available developer [19]:

$$s_{ijk} = 1 - p_{ijk}\, u_k\, (1-\varepsilon), \tag{17}$$

where $u_k \in [0,1]$ is the uniformity parameter. The number of available and developed grains are drawn from compound distributions:

$$\tilde{N}_{ijk} \sim \text{Poisson}\left({}^{N_k}/_{s_{ijk}}\right), \tag{18a}$$

$$X_{ijk} \sim \text{Binomial}\left(\tilde{N}_{ijk},\ p_{ijk}\right), \tag{18b}$$

and the grain density contribution per pixel is

$$g_{ijk} = X_{ijk}\,\frac{D_k^{\max} + d_k^{\min}}{N_k}\,s_{ijk}. \tag{19}$$

A final Gaussian blur of radius r_g pixels models grain clumping within the emulsion layer.

4 Print Exposure and Development

The developed negative encodes scene information as a spatial distribution of CMY dye densities. To produce a positive print, the negative is placed in a color enlarger and its transmitted light is used to expose photographic paper.

4.1 Color-Enlarger Projection

The developed negative density $\mathbf{d}^-$ is converted to spectral transmittance and projected onto photographic paper through a dichroic color-enlarger head.

4.1.1 Spectral density of the negative

The CMY dye-density matrix $\mathbf{Q} \in \mathbb{R}^{L\times 4}$ maps CMY density channels to spectral optical density. Its first three columns contain the absorption spectra of the cyan, magenta, and yellow dye layers, respectively; its fourth column encodes the base-plus-fog spectrum:

$$\Delta_{ij\lambda} = \sum_{k\in\{C,M,Y\}} d^-_{ijk}\, Q_{\lambda k} + Q_{\lambda,4}\, q_{\min}, \tag{20}$$

where $q_{\min}$ scales the minimum-density floor.

Fig. 6: **Flowers:** (left) The original input image, and (right) the output using a Kodak Ultramax 400 negative and a Kodak Supra Endura paper.

4.1.2 Dichroic filter head

The source illuminant $e(\lambda)$ is attenuated through independent Y, M, C filter elements with measured transmittance curves $T_k(\lambda)$. For dial settings $v_k \in [0, 1]$, the combined transmittance is

$$T_{\text{YMC}}(\lambda) = \prod_{k\in\{Y,M,C\}} \left[1 - (1 - T_k(\lambda))\, v_k\right], \tag{21}$$

and the filtered illuminant is $e'(\lambda) = e(\lambda)\, T_{\text{YMC}}(\lambda)$.

4.1.3 Mid-grey normalization

The scalar η anchors scene mid-grey to paper mid-grey. An 18% grey patch is traced through the camera–film–enlarger chain using only the H&D curve mapping (no grain or DIR-coupler corrections) to obtain a noise-free reference signal:

$$\eta = \frac{1}{R^{p,\text{grey}}_{\text{green}}}, \tag{22}$$

where $R^{p,\text{grey}}_{\text{green}}$ is the green-channel paper exposure produced by the grey patch under Eq. (23) with $\eta = 1$.

4.1.4 Paper raw exposure

The light transmitted through the negative is integrated against the paper sensitivity $\mathbf{s}^p \in \mathbb{R}^{L\times 3}$:

$$R^p_{ijk} = \tau_{\text{print}}\, \eta \int_\Lambda 10^{-\Delta_{ij}(\lambda)}\, e'(\lambda)\, s^p_k(\lambda)\, \mathrm{d}\lambda, \tag{23}$$

where τ_{print} is a user-input paper exposure multiplier. The term $10^{-\Delta_{ij}(\lambda)}$ converts the negative's spectral optical density to transmittance via the Beer–Lambert law. The paper H&D stage (Section 3.3) then receives the log-exposure $H^p_{ijk} = \log_{10} R^p_{ijk}$.

4.2 Paper Development and Scanning

Photographic paper is developed by applying the H&D curve mapping (Eq. 8) to the log-exposure H^p, omitting grain and DIR-couplers, to yield a CMY density image $\mathbf{d}^p$.

Fig. 7: **VW Bus:** (left) The original input image, and (right) the output using a Fujifilm C200 negative and a Kodak Endura Premier paper.

The final RGB image is produced by illuminating the paper density under a viewing illuminant $e^v(\lambda)$ and integrating against the CIE 1931 2° color-matching functions $\bar{x}, \bar{y}, \bar{z}$ [22], [23]:

$$XYZ_{ij} = \frac{1}{N_v} \int_\Lambda 10^{-\Delta^p_{ij}(\lambda)}\, e^v(\lambda) \begin{bmatrix} \bar{x}(\lambda) \\ \bar{y}(\lambda) \\ \bar{z}(\lambda) \end{bmatrix} \mathrm{d}\lambda, \tag{24}$$

$$N_v = \int_\Lambda e^v(\lambda)\, \bar{y}(\lambda)\, \mathrm{d}\lambda. \tag{25}$$

The XYZ values are converted to an output RGB image via a chromatic-adaptation transform from the white point of e^v to D65, followed by the standard XYZ-to-sRGB transform.

5 Results

5.1 Implemenation Details

Our python implementation relies on the python package `colour-science` [24] for various color conversion functions (Mallet-Yuksel basis functions, CIE 1931 2° color-matching, etc). The pipeline builds on [1] as a reference implementation. All input images were taken from `https://www.pexels.com`, with the exception parrot image (Figure 2).

5.2 Visual Results

In addition to the teaser figure (Figure 1) and the flowchart figure (Figure 2), the output images shown in Figures 6–9 demonstrate that the pipeline captures characteristic analog qualities across a range of images. Figure 10 shows that qualitatively, the paper choice makers a bigger difference than the negative for the final color character. This makes sense since the paper H&D curves determine the density-to-color mapping of the positive print, whereas the negative primarily controls which tonal information is passed through.

6 Conclusion

We presented a physically grounded, end-to-end emulation pipeline for emulating the look of analog color photography. Starting from a linear RGB image, our model traces the full darkroom process, with each stage derived from first principles and parameterized by physically meaningful quantities. Qualitative results confirm that the two-stage negative–print architecture captures the characteristic look of analog photography.

Fig. 8: **Bookshelf:** (left) The original input image, and (right) the output using a Fujifilm C200 negative and a Kodak Ektacolor Edge paper.

Fig. 9: **Candles:** (left) The original input image, and (right) the output using a Fujifilm Pro 400H negative and a Fujifilm Crystal Archive paper. Note the strong halation effect from the flames in the output.

6.1 Limitations and Future Work

Our project has several limitations that suggest directions for future work. The pipeline at its current stage can be slow for larger images; future work should explore optimizations to achieve real-time or near-real-time performance. Additionally, a graphical user interface would be useful for interactively adjusting parameters to obtain the desired look. Our grain simulation, while superior to naive white noise, is still a simple approximation; it could be improved by integrating the full stochastic model of [10] into the pipeline. Several analog phenomena are not yet modeled, such as adjacency effects, crossover color balance of shadows and highlights, and spectral shifts in paper dyes under different viewing illuminants. Modeling these effects could further enhance the realism of the output.

References

[1] A. Volpato, "Agx emulsion," https://github.com/andreavolpato/agx-emulsion.git, 2025.

[2] C. Kolb, D. Mitchell, and P. Hanrahan, "A realistic camera model for computer graphics," in *Proceedings of the 22nd annual conference on Computer graphics and interactive techniques*, 1995, pp. 317–324.

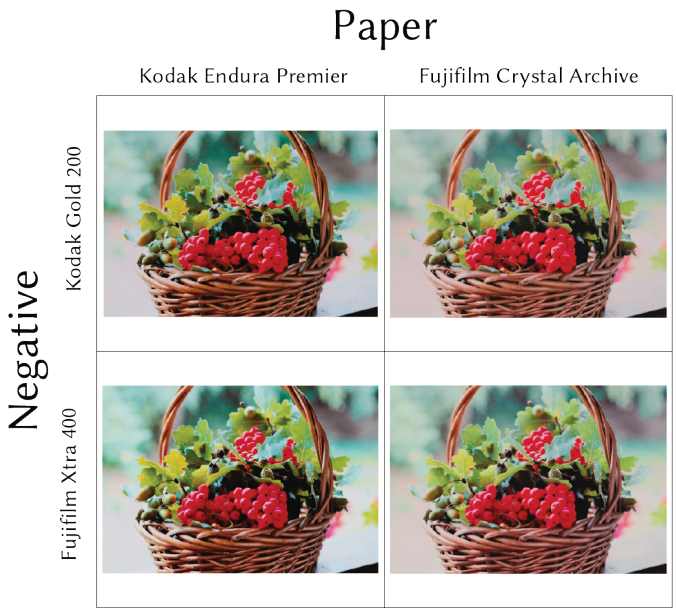

Fig. 10: **The effect of the negative vs. the paper:** Qualitatively, we observe that the paper choice has a much more pronounced effect on color than the negative choice. This is consistent with the paper's H&D curves spanning a wider dynamic range and exhibiting stronger color channel separation than the negative.

[3] J. E. Farrell, P. B. Catrysse, and B. A. Wandell, "Digital camera simulation," *Appl. Opt.*, vol. 51, no. 4, pp. A80–A90, Feb 2012. [Online]. Available: https://opg.optica.org/ao/abstract.cfm?URI=ao-51-4-A80

[4] A. Hertzmann, C. E. Jacobs, N. Oliver, B. Curless, and D. H. Salesin, *Image Analogies*, 1st ed. New York, NY, USA: Association for Computing Machinery, 2001. [Online]. Available: https://doi.org/10.1145/3596711.3596770

[5] B. Wang, Y. Yu, T.-T. Wong, C. Chen, and Y.-Q. Xu, "Data-driven image color theme enhancement," *ACM Trans. Graph.*, vol. 29, no. 6, Dec. 2010. [Online]. Available: https://doi.org/10.1145/1882261.1866172

[6] B. Wang, Y. Yu, and Y.-Q. Xu, "Example-based image color and tone style enhancement," *ACM Trans. Graph.*, vol. 30, no. 4, Jul. 2011. [Online]. Available: https://doi.org/10.1145/2010324.1964959

[7] L. A. Gatys, A. S. Ecker, and M. Bethge, "Image style transfer using convolutional neural networks," *Proceedings of the IEEE Conference on Computer Vision and Pattern Recognition (CVPR)*, pp. 2414–2423, 2016.

[8] D. Ulyanov, V. Lebedev, A. Vedaldi, and V. Lempitsky, "Texture networks: feed-forward synthesis of textures and stylized images," in *Proceedings of the 33rd International Conference on International Conference on Machine Learning - Volume 48*, ser. ICML'16. JMLR.org, 2016, p. 1349–1357.

[9] J. Johnson, A. Alahi, and L. Fei-Fei, "Perceptual losses for real-time style transfer and super-resolution," 2016. [Online]. Available: https://arxiv.org/abs/1603.08155

[10] A. Newson, J. Delon, and B. Galerne, "A stochastic film grain model for resolution-independent rendering," *Computer Graphics Forum*, vol. 36, no. 8, pp. 684–699, 2017. [Online]. Available: https://onlinelibrary.wiley.com/doi/abs/10.1111/cgf.13159

[11] A. Newson, N. Faraj, B. Galerne, and J. Delon, "Realistic film grain rendering," *Image Processing On Line*, vol. 7, pp. 165–183, 2017.

[12] J. Geigel and F. K. Musgrave, "A model for simulating the photographic development process on digital images," in *Proceedings of the 24th Annual Conference on Computer Graphics and Interactive Techniques*, ser. SIGGRAPH '97. USA: ACM Press/Addison-Wesley Publishing Co., 1997, p. 135–142. [Online]. Available: https://doi.org/10.1145/258734.258813

[13] J. I. Echevarria, G. Wilensky, A. Krishnaswamy, B. Kim,

and D. Gutierrez, "Computational simulation of alternative photographic processes," *Computer Graphics Forum*, vol. 32, no. 4, pp. 7–16, 2013. [Online]. Available: https://onlinelibrary.wiley.com/doi/abs/10.1111/cgf.12146

[14] C. A. Porter and G. Spitteler, "Development-inhibitor-releasing (DIR) couplers in photography," *Photographic Science and Engineering*, vol. 13, no. 2, pp. 74–81, 1969.

[15] S. Fujita, "DIR couplers and related compounds," in *Organic Chemistry of Photography*. Berlin, Heidelberg: Springer, 2004, ch. 13.

[16] Dehancer Team, "Dehancer film emulation plugin," 2024, commercial software. [Online]. Available: https://www.dehancer.com/

[17] I. Mallett and C. Yuksel, "Spectral primary decomposition for rendering with srgb reflectance." in *EGSR (DL/I)*, 2019, pp. 9–15.

[18] F. Hurter and V. C. Driffield, "Photo-chemical investigations and a new method of determination of the sensitiveness of photographic plates," *Journal of the Society of Chemical Industry*, vol. 9, pp. 455–469, 1890.

[19] C. E. K. Mees and T. H. James, *The Theory of the Photographic Process*, 3rd ed. New York: Macmillan, 1966.

[20] A. Newson, N. Faraj, J. Delon, and B. Galerne, "Realistic film grain rendering," *Image Processing On Line*, vol. 7, pp. 165–183, 2017.

[21] B. Galerne, A. Newson, and J. Delon, "A stochastic film grain model for resolution-independent rendering," *Computer Graphics Forum*, vol. 36, no. 8, pp. 335–345, 2017.

[22] Commission Internationale de l'Éclairage, "Colorimetry, 3rd edition," CIE, Vienna, Austria, Tech. Rep. CIE 015:2004, 2004.

[23] ——, "Colour-matching functions of CIE 1931 standard colorimetric observer," CIE, Tech. Rep. CIE 018:2019, Table 6, 2019.

[24] Colour & Vision Research Laboratory and Contributors, "Colour — a colour science package for Python," 2023. [Online]. Available: https://www.colour-science.org